Exploring the hypothesis of an inverted Z gradient inside Jupiter

Howard, S.; Guillot, T.; Markham, S.; Helled, R.; Müller, S.; Stevenson, D.J.; ... ; Nettelmann, N.

Astronomy & Astrophysics

Exploring the hypothesis of an inverted *Z* gradient inside Jupiter

S. Howard[1], T. Guillot[1] , S. Markham[1], R. Helled[2], S. Müller[2], D. J. Stevenson[3], J. I. Lunine[4,5] ,
Y. Miguel[6,7], and N. Nettelmann[2]

[1] Université Côte d'Azur, Observatoire de la Côte d'Azur, CNRS, Laboratoire Lagrange, France
   e-mail: `saburo.howard@oca.eu`
[2] Institute for Computational Science, Center for Theoretical Astrophysics & Cosmology, University of Zurich, Winterthurerstr. 190,
   8057 Zurich, Switzerland
[3] Division of Geological and Planetary Sciences, California Institute of Technology, Pasadena, CA 91125, USA
[4] Department of Astronomy, Cornell University, 122 Sciences Drive, Ithaca, NY 14853, USA
[5] Carl Sagan Institute, Cornell University, 122 Sciences Drive, Ithaca, NY 14853, USA
[6] SRON Netherlands Institute for Space Research, Niels Bohrweg 4, 2333 CA Leiden, The Netherlands
[7] Leiden Observatory, University of Leiden, Niels Bohrweg 2, 2333 CA Leiden, The Netherlands

ABSTRACT

Context. Reconciling models of Jupiter's interior with measurements of the atmospheric composition still poses a significant challenge. Interior models favour a subsolar or solar abundance of heavy elements, *Z*, whereas atmospheric measurements suggest a supersolar abundance. One potential solution may be to account for the presence of an inverted *Z* gradient, namely, an inward decrease of *Z*, which implies a higher heavy-element abundance in the atmosphere than in the outer envelope.
Aims. We investigate two scenarios in which the inverted *Z* gradient is either located at levels where helium rain occurs (~Mbar) or at higher levels (~kbar) where a radiative region could exist. Here, we aim to assess the plausibility of these scenarios.
Methods. We calculated interior and evolution models of Jupiter with such an inverted *Z* gradient and we set constraints on its stability and formation.
Results. We find that an inverted *Z* gradient at the location of helium rain is not feasible, as it would require a late accretion and would involve too much material. We find interior models with an inverted *Z* gradient at upper levels due to a radiative zone preventing downward mixing, could satisfy the current gravitational field of the planet. However, our evolution models suggest that this second scenario cannot be validated.
Conclusions. We find that an inverted *Z* gradient in Jupiter could indeed be stable, however, its presence either at the Mbar or kbar levels is rather unlikely.

Key words. planets and satellites: interiors – planets and satellites: gaseous planets

1. Introduction

Models of Jupiter's interior based on Juno gravity data (Durante et al. 2020) have struggled to achieve an agreement with measurements of the atmospheric composition (Li et al. 2020; Wong et al. 2004; Mahaffy et al. 2000). So far, interior models have succeeded in bridging the gap, not without difficulty, by relying on different assumptions, for instance: assuming (albeit not comfortably) a higher entropy in the interior or modifying the equation of state (EOS; Nettelmann et al. 2021; Miguel et al. 2022; Howard et al. 2023), optimising the wind profile (Militzer et al. 2022), or including a decrease of the heavy element abundance *Z* with depth (Debras & Chabrier 2019). The last scenario is described by a so-called inverted *Z* gradient. Interior models actually favour a low metallicity in the outer envelope (subsolar or solar), while atmospheric measurements from *Galileo* and Juno suggest a supersolar abundance of heavy elements (around three times the protosolar value; see e.g. Guillot et al. 2023; Howard et al. 2023). This raises the question of whether the composition measured in the atmosphere is representative of the entire molecular envelope of Jupiter (Helled et al. 2022).

In Sect. 2, we discuss the concept of an inverted *Z* gradient and the constraints it involves in terms of stability and

external accretion. We go on to present two scenarios. First, we assess in Sect. 3, the hypothesis of an inverted *Z* gradient located where helium phase separates, as already proposed by Debras & Chabrier (2019). Second, in Sect. 4, we present a scenario with a similar inverted *Z* gradient but at upper regions, due to a radiative zone.

2. Inverted *Z* gradient: stability and formation

Interior models of Jupiter aim to match the measured gravitational moments that depend on the density distribution of the planet (see, e.g. Zharkov & Trubitsyn 1978). However, the difficulties related to these models in satisfying the gravitational moments indicates that they seem too dense, especially in outer regions of the envelope (0.1–1 Mbar), which have a significant contribution to the gravitational moments. Therefore, an inward-decrease of the heavy element content, in agreement with the supersolar atmospheric measurements but then reduced to solar or subsolar at depths, appears to be a promising idea. Such an inverted *Z* gradient was proposed by Debras & Chabrier (2019). Here, we discuss latter in the following section.

Nevertheless, an inverted *Z* gradient requires it to be stable against convection to be sustained. It can be balanced either

by an increase in the helium mass fraction, Y, or a decrease in temperature to make sure that the density ρ still increases with depth. We estimate, for Jupiter, the maximum increase in heavy elements that can be afforded by increasing Y or by decreasing temperature. To do so, we first calculate $\Delta Z/\Delta Y$ by equating $\rho(Z_j, Y_j)$ and $\rho(Z_{j+1}, Y_{j+1})$, where $\Delta Z = Z_j - Z_{j+1}$ and $\Delta Y = Y_{j+1} - Y_j$ (so that both ΔZ and ΔY have positive values) and then we calculate $\Delta Z/(\Delta T/T)$ by equating $\rho(Z_j, T_j)$ and $\rho(Z_{j+1}, T_{j+1})$, where $\Delta T = T_j - T_{j+1}$ is the temperature difference relative to an isentrope. Here, j refers to the layer where the inverted Z gradient takes place. Densities are calculated using the additive volume law and including non-ideal mixing effects (Howard & Guillot 2023):

$$\frac{1}{\rho(P,T)} = \frac{X}{\rho_{\mathrm{H}}(P,T)} + \frac{Y}{\rho_{\mathrm{He}}(P,T)} + XYV_{\mathrm{mix}} + \frac{Z}{\rho_{\mathrm{Z}}(P,T)}, \quad (1)$$

where $\rho_{\mathrm{H}}, \rho_{\mathrm{He}}, \rho_{\mathrm{Z}}$ are the densities of hydrogen, helium and heavy elements respectively, X, Y, Z their respective mass fractions and V_{mix} is the volume of mixing due to hydrogen-helium interactions. Figure 1 shows the results. In the ideal gas regime in Jupiter, we expect $\Delta Z/\Delta Y \sim 0.5$, meaning that the increase in He is required to be at least twice larger than the change in Z. We also expect $\Delta Z/(\Delta T/T) \sim 0.9$. It is not exactly 1 because we here assumed a mixture of hydrogen and helium consistent with *Galileo*'s measurement of Y (von Zahn et al. 1998). Using an ideal gas relationship of $\Delta\mu/\mu = \Delta T/T$ and the definition of the mean molecular weight of $\frac{1}{\mu} = \frac{X}{\mu_{\mathrm{H}}} + \frac{Y}{\mu_{\mathrm{He}}} + \frac{Z}{\mu_{\mathrm{Z}}}$, we indeed obtain:

$$\Delta Z = \frac{\Delta\mu}{\mu} \times \left(\frac{\mu_{\mathrm{Z}}\mu_{\mathrm{H}}}{\mu_{\mathrm{Z}} - \mu_{\mathrm{H}}} \left(\frac{X}{\mu_{\mathrm{H}}} + \frac{Y}{\mu_{\mathrm{He}}} \right) \right) \sim \frac{\Delta T}{T} \times 0.9, \quad (2)$$

where μ_{H}, μ_{He}, and μ_{Z} are the molecular weights of hydrogen, helium, and heavy elements, respectively. The ideal gas regime extends down to the ~kbar level. Deeper, non-ideal effects kick in and for instance a bigger decrease in temperature is required to allow an inverted Z gradient at deeper regions. We can thus find out how much Z can be balanced by an increase in Y or a decrease in temperature at different levels in Jupiter.

An inverted Z gradient can be stabilised, but vertical transport of heavy material through the stable region may still occur during the lifetime of Jupiter. We know, for example, that breaking gravity waves (Dörnbrack 1998) and Kelvin–Helmholtz instabilities in the Earth's stratosphere produce an eddy diffusion coefficient of 10^3 cm^2 s^{-1} (Massie & Hunten 1981). We assume an eddy diffusion coefficient K_{zz} of 1 cm^2 s^{-1} which is three order of magnitude smaller, but two orders of magnitude larger than the lower bound, molecular diffusivity. In the case of the presence of a radiative zone (discussed in Sect. 4), we consider a thickness L of 1000 km for the stable layer. We obtain a diffusion timescale of:

$$\tau_{\mathrm{mix}} \sim 320\,\mathrm{Myr} \left(\frac{1\,\mathrm{cm}^2\,\mathrm{s}^{-1}}{K_{\mathrm{zz}}} \right) \left(\frac{L}{1000\,\mathrm{km}} \right)^2. \quad (3)$$

A large uncertainty exists on the eddy diffusion coefficient as well as on the thickness of the stable layer, but maintaining this inverted Z gradient on a billion year timescale is rather challenging. In the case of an inverted Z gradient located, where the He phase separates (discussed in Sect. 3), the thickness of the stable region may be greater, increasing the diffusion timescale to the order of one to ten billion years.

Furthermore, this inverted Z gradient implies some constraints on its origin. First, an enrichment from below is ruled out as internal mixing will tend to homogenise the envelope
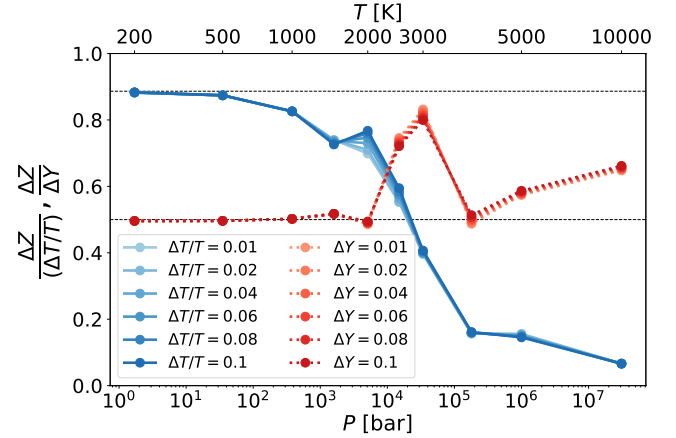

Fig. 1. $\Delta Z/\Delta Y$ and $\Delta Z/(\Delta T/T)$ as a function of pressure and temperature in Jupiter. This shows the maximum increase in heavy elements allowed by increasing Y or by lowering the temperature to ensure stability where the inverted Z gradient takes place. The horizontal dashed lines show the values of $\Delta Z/\Delta Y$ (bottom) and $\Delta Z/(\Delta T/T)$ (top) for an ideal gas. We stress that the calculation of ΔZ has here been done using the HG23+CMS19 EOS (Chabrier et al. 2019; Howard & Guillot 2023) for H–He and the SESAME-drysand EOS (Lyon & Johnson 1992) for heavy elements. The 1 bar temperature was taken at 170 K.

(Vazan et al. 2018; Müller et al. 2020; Müller & Helled 2023). The enrichment hence needs to be external in order to establish an inverted Z gradient. We discuss two important aspects of this external enrichment: the amount and the properties of the accreted material. We show in Fig. 2 how much material can be accreted on Jupiter, through impacts from the destabilised population of the primordial Kuiper belt (Bottke et al. 2023). The estimate of the collisional history was based on constraints derived from the craters found on giant planet satellites and the size-frequency distribution of the Jupiter Trojans. The figure also shows the pressure level in Jupiter at which the accretion of such amount of material would lead to a region above this level, where Z is three times solar. For instance, in the first 500 Myr after Jupiter's formation, about 2×10^{-3} $M_{\oplus}$ can be accreted, which can lead to a threefold enhancement relative to solar from the top of the atmosphere down to 1 kbar. The two scenarios presented in the following sections will have to satisfy this constraint on the possible amount of accreted material. The occurrence of impacts (large impact or cumulative small impacts) to form an inverted Z gradient and an investigation of the stability of this region over billions of years is presented in Müller & Helled (2023).

Finally, we show in Fig. 3 the isotopic ratios of ^{15}N/^{14}N and D/H for objects of the solar system. Only Jupiter (and Saturn) exhibits a protosolar composition of ^{15}N/^{14}N (Guillot et al. 2023) and D/H, while all other present objects have supersolar isotopic ratios. Hence, without an early establishment of the inverted Z gradient, Jupiter's enrichment in heavy elements would have resulted from objects with significantly different isotopic compositions. We would expect the characteristics of a late accretion of heavy elements to match those of objects still present in the Solar System today. This constitutes an additional constraint on the accreted material properties. The argument about isotopes is valid only if we consider that the formed inverted Z gradient involves nitrogen. There is a possibility where the accreted material mostly brought carbon and not nitrogen. In fact, the C/N ratio in comet 67P/Churyumov–Gerasimenko is about 29 (Fray et al. 2017), on average, from dust particles, implying a deficit in nitrogen. Combining this value to gas phase measurements, Rubin et al. (2019)
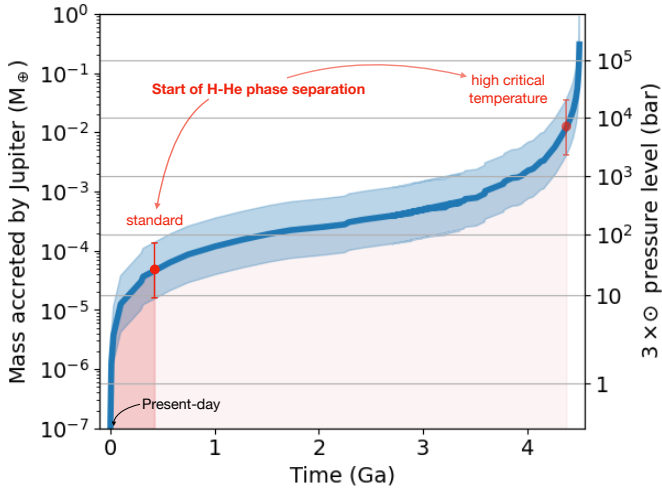
Fig. 2. Accretion of material on Jupiter as a function of time from the present (0) to Jupiter's formation 4.5 Ga ago, based on Bottke et al. (2023). In the last one billion years, Jupiter accreted only about $10^{-4}\,M_\oplus$ of material. The right-hand y axis indicates the pressure levels within Jupiter at which the accretion of material would result in a region above the pressure threshold where Z is three times solar. The time at which H–He phase separation started according either to standard models (e.g., Schöttler & Redmer 2018) or to experiments indicating a high critical temperature (Brygoo et al. 2021) are shown in red. The corresponding error bars correspond to the mass accreted since that time.

found a C/N ratio of 22 and 26 in 67P, considering a dust-to-ice ratio of 1 or 3. The representativity of this C/N ratio value among other comets is an ongoing research area. The C/N ratio of 67P is in line with 1P/Halley (Jessberger et al. 1988) and the lower range of 81P/Wild 2 (de Gregorio et al. 2011). It is also compatible with the chondritic value but large variations are observed in ultracarbonaceous Antarctic micrometeorites (see Engrand et al. 2023). We also stress that the N_2 content of comets may have been lost over time. Yet, if the accreted material was depleted in nitrogen, explaining the formation of an inverted Z gradient would then require to invoke different processes for different components and lead to a C/N value in Jupiter's atmosphere that is close to protosolar ($\sim$4.3, see Table 2 in Guillot et al. 2023). However, we note that uncertainties remain with respect to the composition of the accreted material in both the gaseous and solid phase as well as on the accretion rates.

3. An inverted Z gradient at the helium rain location

One of the only attempts that has succeeded to yield a supersolar abundance of heavy elements in the atmosphere ($Z = 0.02$) was from Debras & Chabrier (2019). These authors included a decrease of heavy elements with depth near He phase separation. It helped reconciling Juno's measurements as it led to lower values of $|J_4|$ and $|J_6|$. To ensure that denser material does not lie on top of lighter material, the decrease in Z was balanced by an increase in Y. Debras & Chabrier (2019) set the phase separation around 0.1 Mbar in their models, where $\Delta Z \sim 0.015$ and ΔY is between $\sim$[0.02−0.05]. Hence, those models have ΔZ between $\sim$[0.3−0.75] $\times \Delta Y$, ensuring a fair level of stability, as Fig. 1 shows that ΔZ needs to be smaller than $\sim$0.6 $\times \Delta Y$ at this pressure level.

However, one of the main explanations for this inverted Z gradient could be the late accretion of heavy material. This scenario requires such accretion to happen after He demix-
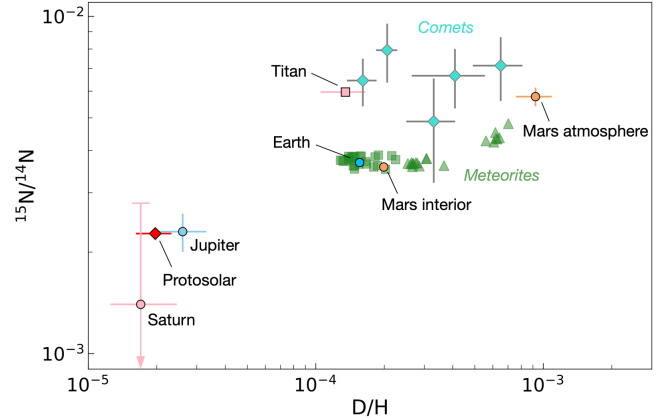

Fig. 3. Isotopic ratios of ^{15}N/^{14}N and D/H among objects from the solar system. Adapted and updated from Marty (2012) and Füri & Marty (2015). The D/H of the interior of Mars is a lower limit. The ^{15}N/^{14}N value of Saturn is only an upper limit, the central point has been chosen at half that value for illustration purposes. Additional details and used references can be found in Appendix B.

ing occurred in Jupiter, so that the accreted material remains above the location of helium rain. Figure 2 shows that to obtain $Z = 3 \times \odot$ above 0.1 Mbar, an accretion of $\sim$0.15 $M_\oplus$ of heavy elements is required. Accreting this amount of material is more likely to occur during the early phases of the Solar System evolution. More realistic values of the pressure at which He phase separates, namely, a few Mbar (Morales et al. 2013; Schöttler & Redmer 2018) indicate that a few $M_\oplus$ of heavy elements are needed to be accreted, which could not be explained. Yet the timing of the scenario put forward by Debras & Chabrier (2019) is challenging. We ran simple evolutionary models of Jupiter (with $M_{\rm core} = 10\,M_\oplus$ and a homogeneous envelope of solar composition). The results are shown in Fig. 4. We find that He phase separation is expected to occur late in the evolution of Jupiter, that is, at 4 Gyr (consistent with Mankovich & Fortney 2020) according to the immiscibility curve of Schöttler & Redmer (2018). Yet it could occur after 100 Myr at the earliest, if we consider the experimental immiscibility curve from Brygoo et al. (2021). In any case, He demixing is happening relatively late. Such late accretion could not bring more than about 0.01 $M_\oplus$ of heavy material (see Fig. 2) and would lead to an enrichment with the wrong isotopic composition, as discussed in Sect. 2.

To salvage this scenario, a giant impact between Jupiter and a Mars-mass object could be envisioned. Such objects are not found in the current Kuiper belt population. Evaluating the likelihood of such an impact at different ages is crucial. Based on conventional H–He phase diagrams, this impact should have occurred very late, in the last 500 Myr, making it an extremely low-probability event. It might also have occurred earlier, as suggested by the high critical demixing temperature of Brygoo et al. (2021). In both cases, however, the impactor should have brought little nitrogen or had a different composition from the observed small objects in the solar system.

4. An inverted Z gradient at uppermost regions due to a radiative zone

We go on to envision an inverted Z gradient located at upper regions ($\sim$kbar) and established early on (less than 10 Myr). Our hypothesis is that the presence of a radiative zone
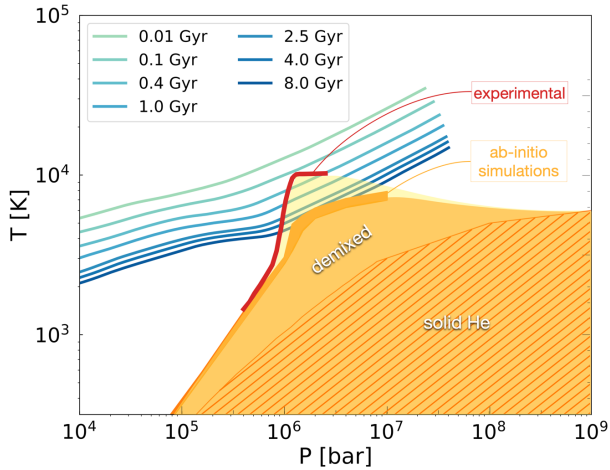
Fig. 4. Sequence in evolutionary time of Jupiter interior profiles (from 10 Myr to 8 Gyr) superimposed with a miscibility diagram of H–He. We show the immiscibility curve of experiments from Brygoo et al. (2021) in red and of ab initio simulations from Schöttler & Redmer (2018) in orange. The hashed region is where He becomes solid.

Fig. 5. J_6 versus J_4 of models including a radiative zone (Z being 3× protosolar above), using the MH13* (Militzer & Hubbard 2013) or HG23+CMS19 (Chabrier et al. 2019; Howard & Guillot 2023) EOS. These models are compared to results by Howard et al. (2023) with no radiative zone nor inverted Z gradient (with Z being only 1.3× protosolar in the atmosphere). The full co-variations of the MCMC calculation using MH13* are given in Appendix A. The circled J shows the Juno measurements (Durante et al. 2020) and the error bar accounts for differential rotation, as in Miguel et al. (2022).

prevents downward mixing. A radiative region could exist in the upper envelope, between 1200 and 2900 K as suggested by Guillot et al. (1994) or between 1400 and 2200 K according to Cavalié et al. (2023). A depletion of alkali metals would bring support to the existence of a radiative layer (Bhattacharya et al. 2023). Accreted heavy material on top of this radiative zone may thus be prevented from mixing with the rest of the envelope below this radiative zone. We note that the presence of a radiative zone is a separate question of getting a higher Z value above this radiative layer, which is what we focus on here.

First we asked whether we could find interior models with a radiative zone that would satisfy the present gravity field measured by Juno. To answer this question, we used the opacities from Guillot et al. (1994), including absorption by H_2, He, H_2O, CH_4, and NH_3 to set a radiative region and implement an inverted Z gradient. Figure 1 shows that an inverted Z gradient can be stabilised by a sub-adiabatic temperature gradient. Around the ~kbar level, ΔZ needs to be smaller than about $0.7 \times \Delta T/T$. Here, our models have $\Delta T/T$ of about 10%, allowing for an increase of Z of three times the protosolar value ($Z \sim 5\%$) (Asplund et al. 2021), thus ensuring stability. We ran Markov chain Monte Carlo (MCMC) calculations, as in Miguel et al. (2022) and Howard et al. (2023). At first, we could not find models that would fit the equatorial radius and the gravitational moments of Jupiter. In this case, the radiative zone was extending from 1200 to 2100 K. We then parameterised (arbitrarily multiplying by 5) the opacities and we could obtain solutions with a radiative region extending from about 1600 to 2100 K. Thus, the possible location and extent of the radiative zone may be constrained by the gravity data. Figure 5 shows the gravitational moments J_4 and J_6 of these models, for two EOSs (the full posterior distributions are given in Appendix A for one EOS). We find that interior models that include such a radiative zone can satisfy the observed gravitational moments from Juno (at 3σ in J_6) as well as the compositional constraints on the atmosphere.

To get $Z = 3 \times \odot$ above 1 kbar, an accretion of $\sim 2 \times 10^{-3}\,M_\oplus$ of heavy elements is required, which can be done in the first few hundred million years (see Fig. 2). The isotopic constraints mentioned in Sect. 2 imply that a late delivery of heavy material can hardly be possible. Hence, we examine whether the inverted Z
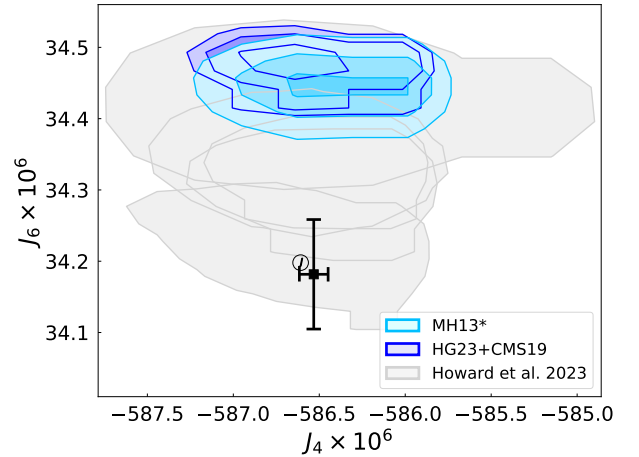
gradient could have been formed early and maintained in Jupiter. To this end, we use again our evolutionary models presented in Sect. 3 and include now a radiative zone using the parameterised opacities. Figure 6 compares the radiative and adiabatic temperature gradients, from 1 Myr to 4 Gyr. The radiative zone is located roughly where the radiative gradient is lower than the adiabatic gradient. The radiative region appears around 10 Myr and is progressively shifted to deeper regions. Thus, the initially enriched material above the radiative zone will progressively mix with material of protosolar composition as the radiative zone is shifted to deeper levels. Such behaviour of the radiative zone was already predicted by Guillot (1999). Considering that the mass above the radiative region at 10 Myr is $\sim 10^{-5}\,M_J$ and increases to $\sim 3.10^{-4}\,M_J$ at 4 Gyr, the Z gradient at 10 Myr must be high enough so that the abundance of heavy elements becomes approximately three times the protosolar value nowadays. If the disk phase does not exceed 10 Myr, a Z value of 60 times the protosolar value ($\Delta Z \sim 0.9$) is required above the radiative zone, at 10 Myr. Keeping such a ΔZ and ensuring stability may be hard since a significant $\Delta T/T$ would be required to prevent mixing (the factor of 0.9 in Eq. (2) would even be lower given the increased molecular weight due to a much higher Z value), making the scenario rather unlikely. Furthermore, diffusion through the radiative zone is expected after a few hundred million years (see Sect. 2), making the scenario even more challenging. However, this behaviour of the radiative zone as the planet evolves is one case corresponding to the use of a specific opacity table and the details of the evolution code. Further investigation of this scenario is therefore required.

5. Conclusion

The inverted Z gradient is an appealing notion for interior models to explain both the gravity field and the atmospheric composition of Jupiter. It may also be of interest to Saturn as reconciling interiors models with the measured metallicity is challenging as well (Mankovich & Fuller 2021), noting that helium
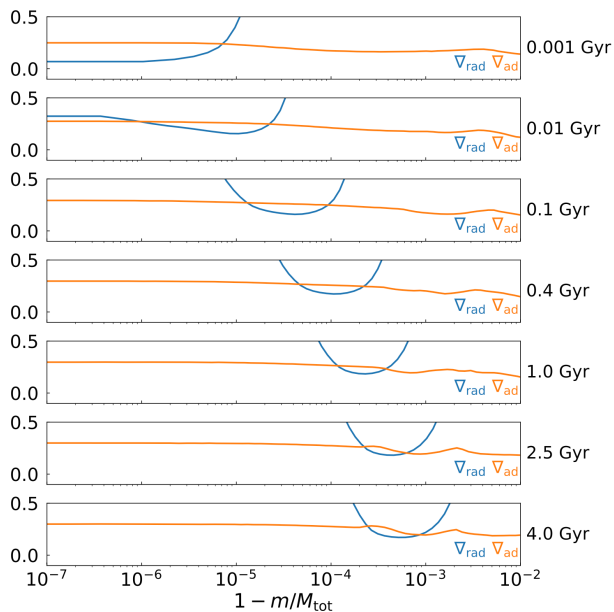
Fig. 6. Comparison of the radiative and adiabatic temperature gradients in Jupiter, at ages ranging from 1 Myr to 4 Gyr. We estimate the minimum value of ∇_{rad} as the approximate upper limit of the radiative region. The evolution models consist of a central core of 10 $M_{\oplus}$ and a homogeneous envelope of solar composition.

rain is expected to start earlier. An inverted Z gradient can be stabilised by either an increase in the helium mass fraction or a decrease in temperature. However, as we show here, such a Z gradient in Jupiter at the location of helium rain, as proposed by Debras & Chabrier (2019), is rather unlikely as it requires to accrete an excessive amount of material, which cannot be justified based on collisional evolution models of the solar system. It also requires a late accretion, which isotopic constraints do not allow. An inverted Z gradient, established early and at upper regions (~kbar), due to a radiative zone, might be a solution. We show that such a scenario works from the point of view of the present gravity data and enough material may be accreted. Nevertheless, this radiative zone appears around 10 Myr and is shifted to deeper regions with time. Such inward-shift of the radiative zone requires, at ~10 Myr, a significant Z gradient ($\Delta Z \sim 0.9$ in our case) that is hard to stabilise. However, our calculations rely on a specific (and parameterised) opacity table used here. Updated opacity data (see e.g. Tennyson & Yurchenko 2012; Freedman et al. 2014) could produce a radiative region at a different location and with a different evolution, changing the required mass that needs to be accreted to enrich the outer envelope. Furthermore, despite this work being based on the latest considerations regarding the quantity and properties of the materials enriching the atmosphere, our knowledge of Jupiter's potential accreted material is still incomplete. Yet, in our setup, the hypothesis of a radiative zone that prevents downward mixing is rather unlikely. Alternative scenarios such as an inverted gradient of helium, instead of heavy elements, as well as further investigations of the topic are required to resolve Jupiter's metallicity puzzle.

References

Abbas, M. M., Kandadi, H., LeClair, A., et al. 2010, ApJ, 708, 342
Aléon, J. 2010, ApJ, 722, 1342
Anders, E., & Grevesse, N. 1989, Geochim. Cosmochim. Acta, 53, 197
Asplund, M., Amarsi, A. M., & Grevesse, N. 2021, A&A, 653, A141
Bhattacharya, A., Li, C., Atreya, S. K., et al. 2023, ApJ, 952, L27
Biver, N., Moreno, R., Bockelée-Morvan, D., et al. 2016, A&A, 589, A78
Bockelée-Morvan, D., Calmonte, U., Charnley, S., et al. 2015, Space Sci. Rev., 197, 47
Bottke, W. F., Vokrouhlický, D., Marshall, R., et al. 2023, PSJ, 4, 168
Brygoo, S., Loubeyre, P., Millot, M., et al. 2021, Nature, 593, 517
Cavalié, T., Lunine, J., & Mousis, O. 2023, Nat. Astron., 7, 678
Chabrier, G., Mazevet, S., & Soubiran, F. 2019, ApJ, 872, 51
Debras, F., & Chabrier, G. 2019, ApJ, 872, 100
de Gregorio, B. T., Stroud, R. M., Cody, G. D., et al. 2011, Meteorit. Planet. Sci., 46, 1376
Dörnbrack, A. 1998, J. Fluid Mech., 375, 113
Durante, D., Parisi, M., Serra, D., et al. 2020, Geophys. Res. Lett., 47, e86572
Engrand, C., Lasue, J., Wooden, D. H., & Zolensky, M. E. 2023, ArXiv e-prints [arXiv:2305.03417]
Fletcher, L. N., Greathouse, T. K., Orton, G. S., et al. 2014, Icarus, 238, 170
Fray, N., Bardyn, A., Cottin, H., et al. 2017, MNRAS, 469, S506
Freedman, R. S., Lustig-Yaeger, J., Fortney, J. J., et al. 2014, ApJS, 214, 25
Füri, E., & Marty, B. 2015, Nat. Geosci., 8, 515
Geiss, J., & Gloeckler, G. 2003, Space Sci. Rev., 106, 3
Guillot, T. 1999, Planet. Space Sci., 47, 1183
Guillot, T., Gautier, D., Chabrier, G., & Mosser, B. 1994, Icarus, 112, 337
Guillot, T., Fletcher, L. N., Helled, R., et al. 2023, ASP Conf. Ser., 534, 947
Helled, R., Stevenson, D. J., Lunine, J. I., et al. 2022, Icarus, 378, 114937
Howard, S., & Guillot, T. 2023, A&A, 672, L1
Howard, S., Guillot, T., Bazot, M., et al. 2023, A&A, 672, A33
Jessberger, E. K., Christoforidis, A., & Kissel, J. 1988, Nature, 332, 691
Kerridge, J. F. 1985, Geochim. Cosmochim. Acta, 49, 1707
Lellouch, E., Bézard, B., Fouchet, T., et al. 2001, A&A, 370, 610
Li, C., Ingersoll, A., Bolton, S., et al. 2020, Nat. Astron., 4, 609
Lis, D. C., Bockelée-Morvan, D., Güsten, R., et al. 2019, A&A, 625, L5
Lyon, S. P., & Johnson, J. D. 1992, LANL Report, LA-UR-92-3407
Mahaffy, P. R., Donahue, T. M., Atreya, S. K., Owen, T. C., & Niemann, H. B. 1998, Space Sci. Rev., 84, 251
Mahaffy, P. R., Niemann, H. B., Alpert, A., et al. 2000, J. Geophys. Res., 105, 15061
Manfroid, J., Jehin, E., Hutsemékers, D., et al. 2009, A&A, 503, 613
Mankovich, C. R., & Fortney, J. J. 2020, ApJ, 889, 51
Mankovich, C. R., & Fuller, J. 2021, Nat. Astron., 5, 1103
Marty, B. 2012, Earth Planet. Sci. Lett., 313, 56
Marty, B., Chaussidon, M., Wiens, R. C., Jurewicz, A. J. G., & Burnett, D. S. 2011, Science, 332, 1533
Massie, S. T., & Hunten, D. M. 1981, J. Geophys. Res. Oceans, 86, 9859
Mathew, K. J., & Marti, K. 2001, J. Geophys. Res., 106, 1401
Michael, P. J. 1988, Geochim. Cosmochim. Acta, 52, 555
Miguel, Y., Bazot, M., Guillot, T., et al. 2022, A&A, 662, A18
Militzer, B., & Hubbard, W. B. 2013, ApJ, 774, 148
Militzer, B., Hubbard, W. B., Wahl, S., et al. 2022, Planet. Sci. J., 3, 185
Morales, M. A., Hamel, S., Caspersen, K., & Schwegler, E. 2013, Phys. Rev. B, 87, 174105
Müller, S., & Helled, R. 2023, ApJ, submitted
Müller, S., Helled, R., & Cumming, A. 2020, A&A, 638, A121
Nettelmann, N., Movshovitz, N., Ni, D., et al. 2021, Planet. Sci. J., 2, 241
Niemann, H. B., Atreya, S. K., Demick, J. E., et al. 2010, J. Geophys. Res. (Planets), 115, E12006
Owen, T., Mahaffy, P. R., Niemann, H. B., Atreya, S., & Wong, M. 2001, ApJ, 553, L77
Rubin, M., Altwegg, K., Balsiger, H., et al. 2019, MNRAS, 489, 594
Saito, H., & Kuramoto, K. 2020, ApJ, 889, 40
Schöttler, M., & Redmer, R. 2018, Phys. Rev. Lett, 120, 115703
Shinnaka, Y., Kawakita, H., Jehin, E., et al. 2016, MNRAS, 462, S195
Tennyson, J., & Yurchenko, S. N. 2012, MNRAS, 425, 21
Vazan, A., Helled, R., & Guillot, T. 2018, A&A, 610, L14
von Zahn, U., Hunten, D. M., & Lehmacher, G. 1998, J. Geophys. Res., 103, 22815
Webster, C. R., Mahaffy, P. R., Flesch, G. J., et al. 2013, Science, 341, 260
Wong, M. H., Mahaffy, P. R., Atreya, S. K., Niemann, H. B., & Owen, T. C. 2004, Icarus, 171, 153
Wong, M. H., Atreya, S. K., Mahaffy, P. N., et al. 2013, Geophys. Res. Lett., 40, 6033
Zharkov, V. N., & Trubitsyn, V. P. 1978, Physics of Planetary Interiors, Astronomy and Astrophysics Series (Tucson: Pachart)

Appendix A: Corner plot of models using MH13* and including a radiative zone

Figure A.1 shows the posterior distributions of the MCMC simulations using the MH13* EOS (Militzer & Hubbard 2013), including a radiative zone and an inverted Z gradient.
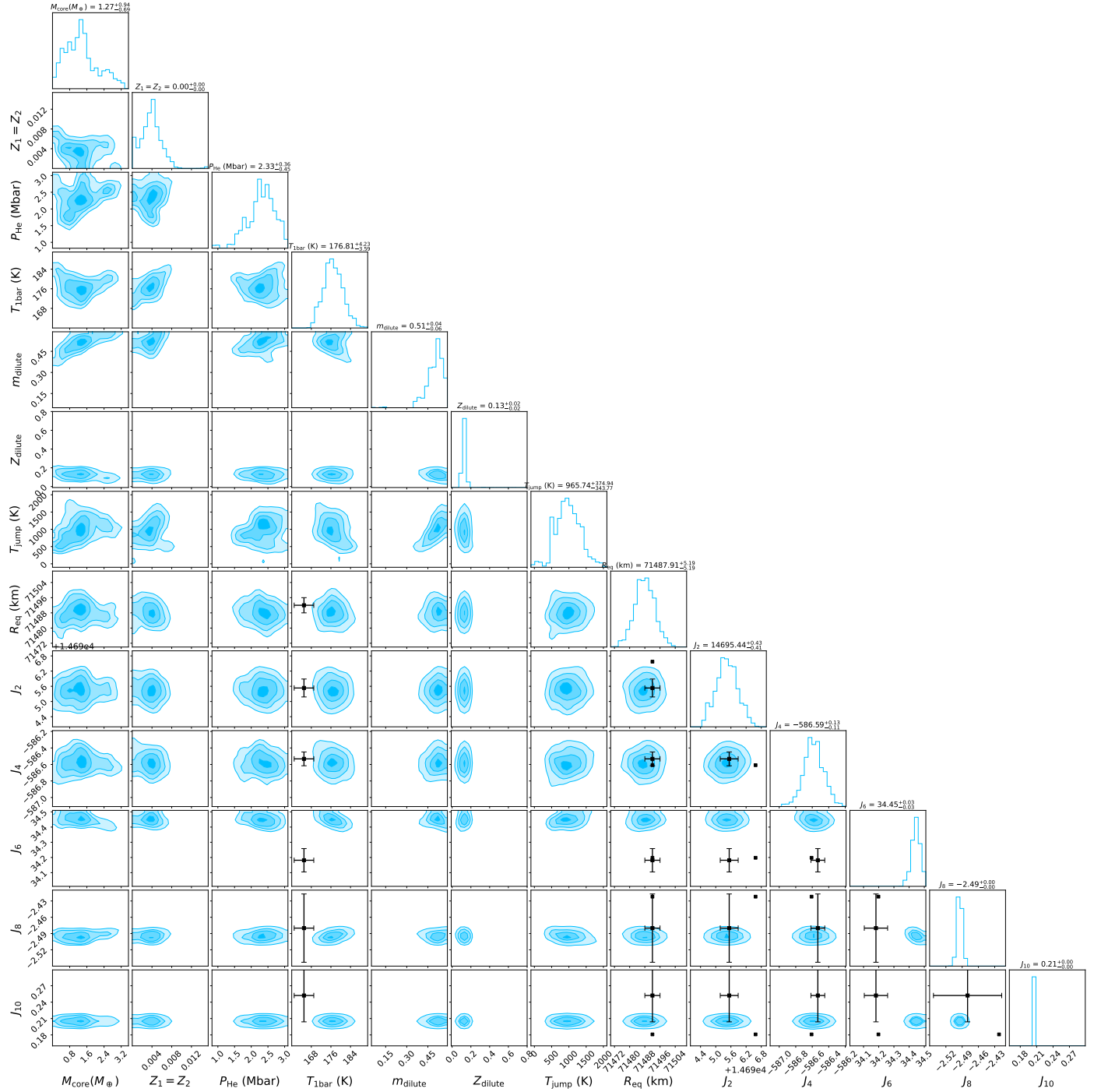

Fig. A.1. Posterior distributions obtained with the MH13* EOS (Militzer & Hubbard 2013), including a radiative zone (opacities multiplied by 5). The black points correspond to the measured J_{2n} by Juno. The black error bars correspond to Juno's measurements accounting for differential rotation for the J_{2n} and Galileo's measurement for T_{1bar}.

Appendix B: Additional details and references for isotopic ratios of $^{15}N/^{14}N$ and D/H used in Fig. 3

This appendix lists the references used to plot the isotopic ratios shown in Fig. 3. Jupiter's data come from Galileo (Mahaffy et al. 1998; Owen et al. 2001): D/H = (2.6±0.7)×10^{-5} and $^{15}N/^{14}N$ = (2.3 ± 0.3) × 10^{-3}. Protosolar values come from Marty et al. (2011), Geiss & Gloeckler (2003). Earth's data come from Anders & Grevesse (1989), Michael (1988). Mars' data come from Mathew & Marti (2001) and Wong et al. (2013), Webster et al. (2013), respectively, for its interior and its atmosphere. The D/H of the interior is a lower limit as large variations are measured in martian meteorites (Saito & Kuramoto 2020). Saturn's data are from Lellouch et al. (2001), Fletcher et al. (2014): D/H = $1.7^{+0.75}_{-0.45} \times 10^{-5}$ and $^{15}N/^{14}N$ = 2.8×10^{-3}. The $^{15}N/^{14}N$ value is an upper limit. Titan's data are from Niemann et al. (2010), Abbas et al. (2010). For meteorites, bulk isotopic ratios (*squares*) and values in insoluble organic matter (IOM) (*triangles*) are displayed. Here are shown data for various types of chondrites (CI, CM, CO, CR, and CV) from Kerridge (1985), Aléon (2010). The data for five comets (103P/Hartly, C/2009 P1 Garradd, C/1995 O1 Hale-Bopp, 8P/Tuttle and C/2012 F6 Lemmon, from left ro right) are displayed, taken from Manfroid et al. (2009), Biver et al. (2016), Shinnaka et al. (2016), Lis et al. (2019) and Bockelée-Morvan et al. (2015) and references therein. We note that the average $^{15}N/^{14}N$ value for 21 comets has been found to be 0.007 ± 0.001 (Manfroid et al. 2009).